AUTONOMOUS SHIP APPROACH AND LANDING USING DYNAMIC INVERSION CONTROL WITH DECK MOTION PREDICTION

Joseph F. Horn and Junfeng Yang, Pennsylvania State University, University Park PA, United States

Chengjian He and Dooyong Lee, Advanced Rotorcraft Technologies, Sunnyvale CA, United States

John K. Tritschler, United States Naval Test Pilot School, Patuxent River, MD, United States

ABSTRACT

This paper presents the design and simulation testing of a control law for autonomous recovery of a rotorcraft to a moving ship. The paper focuses on the final approach, descent, and landing phases of the ship recovery task when the flight deck is moving dynamically due to sea state. The controller design is based on the dynamic inversion method, and it is assumed that the inertial position of the flight deck is measured and available to the controller. The controller is tested and demonstrated using a FLIGHTLAB simulation model of a medium utility helicopter operating on a ship similar to a DDG-51 destroyer. The decelerating approach profile is based on profiles typically used by human pilots. Two different methods are investigated for the landing: 1) deck tracking with a steady decrease in height above deck, and 2) an optimal control approach that uses forecasted deck state as the terminal condition. Deck motion prediction is achieved via a Minor Components Analysis algorithm that uses recorded state history of the deck motion to predict deck state five seconds in the future. Simulation results show the controller performs well in tracking the straight and oblique approach paths, but its performance can be sensitive to path parameters that result in aggressive deceleration. The simple deck tracking approach to landing resulted in surprisingly good performance when tested over 30 randomized cases, but this control strategy results in large amplitude maneuvering in lateral and vertical axes throughout the descent. The predictive landing method showed potential for achieving more efficient landings with less maneuvering, but overall controller performance was less consistent and sensitive to inaccuracies in the deck motion prediction. The deck motion prediction and optimal control methods require further development to provide reliable autonomous landings.

NOTATION

A, B	= linear system and control matrix
K_p, K_d, K_i	= proportional, derivative, and integral gains
p, q, r	= body-axis angular rates
R	= range to flight deck
R_{pd}	= range to peak deceleration
s	= Laplace operator
V	= airspeed
$V_{app}, \gamma_{app}, \psi_{app}$	= approach velocity, approach glideslope, and approach azimuth
V_X, V_Y, V_Z	= helicopter velocities
w	= body-axis vertical velocity
x, y, h	= aircraft position in NEU inertial coordinates
$\delta_{lat}, \delta_{lon}, \delta_{coll}, \delta_{ped}$	= primary control inputs
ϕ, θ, ψ	= helicopter Euler angles
τ	= time constant
ν	= pseudo-control
ω_n, ζ	= natural frequency, damping ratio

Subscripts and superscripts:

cmd	= commanded value
hhf	= helicopter heading frame
m	= model response
N, E	= North, East in inertial frame
shf	= ship heading frame

1. INTRODUCTION

Landing a rotorcraft on a moving ship deck and under the influence of an unsteady ship airwake is extremely challenging. In high sea states, high winds, and degraded visual environment, workload during this task approaches the limits of a human pilot's capability. For large deck motions, maintaining zero relative velocity in the final phases of landing can be problematic as the aircraft approaches limitations on power margin, control authority, and aircraft state (such as attitude) constraints. Alternatively, pilots commonly hold a stable hover in the inertial frame, identify a quiescent period in ship motion, and land when the deck motion is small. This technique can contribute to fatigue and pilot workload while extending the time of the landing task. Advanced control designs that ease or even

automate ship landing have potential to enhance flight safety and expand shipboard flight envelopes.

A number of researchers have investigated the use of ship deck state feedback to augment the response characteristics of the rotorcraft [1, 2]. Significant improvements in handling qualities for a landing task were demonstrated using augmented response types such as ship relative translation rate command, at least for moderate sea states. This level of augmentation requires full-authority fly-by-wire control and advanced sensing systems. Assuming that such systems will be implemented on future rotorcraft, extension to full autonomy becomes a viable option. For example, an autonomous approach controller was developed and tested in simulation using nature inspired tau-gap control [3]. An autonomous helicopter approach and landing system was proposed by Yang and Yuan [4], in which the recovery procedure was broken into two parts – approach and landing, similar to what is proposed in this paper. Trajectory generation was based on a line-of-sight approach and a classical PID control law was used for trajectory tracking. Yang and Yuan also attempted to use deck motion prediction in the descent and landing phase. Recently, Hu et al proposed an adaptive controller and a vision-based deck motion estimator for landing on a vertically moving platform, and they demonstrated components of the system in quad-rotor flight experiments [5].

This paper presents the development of flight control laws and deck motion prediction algorithms to automate the approach and landing task in high sea states. The control implementation assumes that deck states are available to the approaching aircraft (either from on-board sensors or sent from the ship via telemetry, the actual deck state sensing is not within the scope of this paper). The investigation focuses on the final approach and landing phase of the shipboard recovery. The algorithms are demonstrated in high fidelity simulations using the FLIGHTLAB software.

The final landing phase of the ship recovery is considered the most challenging control problem, especially when the flight deck is undergoing large dynamic motion due to sea state. Two approaches were investigated for this phase. First, a simple station-keeping method is used where the controller attempts to hold position over the center of the flight deck while it slowly decreases relative deck height. The method uses direct feedback of the measured flight deck position and velocities in all three axes. This approach is considered the “baseline” case, and is not ideal due to the extensive maneuvering required of the helicopter to track dynamic deck motions. In some cases this approach might become infeasible as the helicopter would not have sufficient bandwidth, power margin, or control authority achieve the necessary maneuvers.

It is hypothesized that a better approach would be to plan a landing trajectory by forecasting the future motion of the deck (something that experienced pilots are able to do). The helicopter could plan a less dynamic descent path that terminates the landing with small relative velocity. Deck motion prediction algorithms are proposed, where past deck state measurements are processed by the algorithm to predict future deck state at some fixed time horizon. A control law based on classical optimal control is used to generate the descent trajectory.

2. SIMULATION ENVIRONMENT

2.1. FLIGHTLAB

For the present study, a high fidelity blade element formulation in FLIGHTLAB was used. FLIGHTLAB is an industry-standard rotorcraft flight dynamics modeling and analysis tool that has been extensively validated and widely used in support of rotorcraft design, analysis, and full flight simulation. FLIGHTLAB adopts a modern object-oriented programming approach and applies a geometrically exact multi-body dynamics formulation that combines with blade element based unsteady aerodynamics modelling for a high-fidelity flight dynamics simulation. FLIGHTLAB provides an extensive modelling element library that covers all the disciplines typically required for rotorcraft flight dynamics modelling, including: 1) structural dynamics, 2) aerodynamics, 3) engine and drivetrain dynamics, and 4) flight controls. A nonlinear full flight simulation model for an arbitrary rotorcraft configuration can be built in FLIGHTLAB by assembling the modelling elements with user-provided physical geometry and structural and aerodynamic property data.

2.2. Medium Utility Helicopter Model

The blade element model represents a generic medium weight (17,000 lbs class) helicopter, with similar dimensions as a UH-60. The model includes rotor flapping and lead-lag dynamics, unsteady airloads, and a high-order Peters-He finite state dynamic wake method for rotor induced flow and interference modelling [6].

The unsteady airloads allow for the effects of blade yawed-flow, pitch rate, and stall delay due to blade rotation [7]. The airframe model consists of a fuselage, empennage, sensor, and landing gear subsystems. The fuselage is modelled using nonlinear 6-DOF dynamics. The fuselage airloads are computed via empirical table look-up as a

function of angle of attack and sideslip. The empennage consists of left and right horizontal stabilators as well as a vertical fin with main rotor wake interference effect. This configuration has a three-wheeled landing gear (left, right, and tail gear) similar to a UH-60. The landing gear is modelled as a nonlinear spring/damper system that interacts with the ship deck once the aircraft touches down. The landing gear also includes a tire model with a two phase (static and dynamic rolling) friction formulation to simulate the interaction with a moving ship deck surface. The simulation also includes a simple sensor model which outputs aircraft body attitude and rate information for use by the flight controls. The flight control laws are implemented using the Control System Graphical Editor (CSGE), which allows control laws to be built in block diagram form and then directly imported to the simulation.

2.3. Ship Environment

The ship dynamics are based on standard deck motion data for a generic surface combatant ship similar to a DDG-51 type destroyer. The database was developed by the U.S. Navy Office of Naval Research and the Naval Surface Warfare Center under the Systematic Characterization of the Naval Environment (SCONE) program [8]. The SCONE data provides three levels of deck motion intensity (low, medium, and high) with dominant motion in either the roll or heave axes. It includes dynamics in all six DOF: surge, sway, heave, roll, pitch and yaw. However, for the current study dynamic surge was not included in the model. For the results in this paper, the medium intensity motion with dominant heave motion was used. Table 1 summarizes the RMS and min/max motion properties. Note that while the deck motion is classified as “moderate”, the heave motion is quite significant, with vertical displacements and velocities as high as 13 ft and 12 ft/sec from the mean.

	Displacement		*Rate (deg/sec or ft/sec)*	
DOF	***RMS***	***Max/Min***	***RMS***	***Max/Min***
Roll	0.94°	3.5°/-4.1°	0.66	3.3 /-2.8
Pitch	0.91°	3.7°/-3.4°	0.89	3.9 / -3.3
Yaw	0.21°	1.2°/-0.7°	0.15	0.49 / -0.58
Sway	2.1 ft	4.3 /-13 ft	0.88	3.3 / -3.7
Heave	2.5 ft	25 /-3.5 ft	2.4	11.7 / -10.8

Table 1 Ship Motion Properties

The ship airwake is modelled with a spatially non-uniformly distributed mean disturbance plus a stochastic turbulent airwake variation [9]. The magnitudes of the non-uniform mean and turbulent variation were derived from a Navier-Stokes based CFD ship airwake solution for a generic ship shape. At the current study, one wind over deck condition was investigated: 20 knots wind over deck, 0° relative wind.

3. DYNAMIC INVERSION CONTROL LAW

The control law was designed based on the dynamic inversion (DI) method. However, many of the concepts used in the approach, deck following, and landing control laws could readily be extended to other control law architectures (such as explicit model following). A schematic of the overall control law is illustrated in Fig. 1. Details of the control algorithms will be presented in the following sections.

3.1. Inner Loop Control Law

The inner loop uses a dynamic inversion control law similar to what was used in previous work [2]. The controller uses a set of reduced order linear models of the helicopter dynamics and inverts these linear models to calculate actuator deflections that track a desired state acceleration. In this study, the inner loop controller is simplified compared to that of Ref. 2. The linear model used for inversion is a 4th order linear system, consisting only of angular rates and vertical velocity:

$$(1)\qquad \begin{bmatrix} \dot{p} \\ \dot{q} \\ \dot{w} \\ \dot{r} \end{bmatrix} = [A] \begin{bmatrix} p \\ q \\ w \\ r \end{bmatrix} + [B] \begin{bmatrix} \delta_{lat} \\ \delta_{long} \\ \delta_{coll} \\ \delta_{ped} \end{bmatrix}$$

This model is a reasonable representation of the short term linear rate dynamics of the helicopter for use in inner loop control. The A and B matrices are based on reduced order linear models extracted directly from the simulation model. Models were extracted at airspeeds from hover to 160 knots in 20 knot increments. The DI control law is then given by:

$$(2)\qquad \begin{bmatrix} \delta_{lat} \\ \delta_{long} \\ \delta_{coll} \\ \delta_{ped} \end{bmatrix} = [B(V)]^{-1} \left(\begin{bmatrix} \nu_p \\ \nu_q \\ \nu_r \\ \nu_w \end{bmatrix} - [A(V)] \begin{bmatrix} p \\ q \\ w \\ r \end{bmatrix} \right)$$

where *A(V)* and *B(V)* denote that these matrices are a function of airspeed. They are scheduled at the airspeeds defined above and linearly interpolated. The ν parameters are the pseudo-controls which

represent the desired accelerations plus PID compensation on the tracking error, as will be described below. If we subsitute the control law, Eq. (2), into the assumed plant dynamics in Eq. (1), we have:

$$\begin{aligned} &\dot{x} = v \\ &\text{where } x = \begin{bmatrix} p & q & w & r \end{bmatrix}^T \\ &v = \begin{bmatrix} v_p & v_q & v_w & v_r \end{bmatrix}^T \end{aligned} \tag{3}$$

Dynamic inversion converts the plant to a set of de-coupled integrators, which can be readily stabilized by adding PID compensation in the pseudo-control vector. The following pseudo-controls were used, where the subscript m denotes the desired state value based on our ideal response model:

$$\begin{aligned} v_\phi &= \ddot{\phi}_m + K_{d\_\phi}(\dot{\phi}_m - \dot{\phi}) + K_{p\_\phi}(\phi_m - \phi) + K_{i\_\phi}\int(\phi_m - \phi)dt \\ v_\theta &= \ddot{\theta}_m + K_{d\_\theta}(\theta_m - \dot{\theta}) + K_{p\_\theta}(\theta_m - \theta) + K_{i\_\theta}\int(\theta_m - \theta)dt \\ v_r &= \dot{r}_m + K_{p\_r}(r_m - r) + K_{i\_r}\int(r_m - r)dt \\ v_w &= -\left(\dot{V}_{Z_m} + K_{p\_VZ}(V_{Z_m} - V_Z) + K_{i\_VZ}\int(V_{Z_m} - V_Z)dt\right) \end{aligned} \tag{4}$$

Note that inner-loop control law regulates Euler angles ϕ and θ, whereas the inversion directly controls body-axis angular rates *p* and *q*. The following transformations are use to transform Euler angle pseudo-commands to appropriate body-axis pseudo-commands:

$$\begin{aligned} v_p &= v_\phi - v_\theta \tan\phi\tan\theta - v_r \tan\theta / \cos\phi \\ v_q &= v_r \tan\phi + v_\theta / \cos\phi \end{aligned} \tag{5}$$

The model responses are governed by simple linear transfer functions. The pitch and roll attitude are second order, for example in roll:

$$\begin{bmatrix} \ddot{\phi}_m \\ \dot{\phi}_m \\ \phi_m \end{bmatrix} = \begin{bmatrix} s^2 \\ s \\ 1 \end{bmatrix} \cdot \frac{\omega_n^2}{s^2 + 2\zeta\omega_n s + \omega_n^2} \cdot \phi_{cmd} \tag{6}$$

Vertical speed and yaw rate model responses follow first order systems:

$$\begin{bmatrix} \dot{r}_m \\ r_m \end{bmatrix} = \begin{bmatrix} s \\ 1 \end{bmatrix} \cdot \frac{1}{\tau s + 1} \cdot r_{cmd} \tag{7}$$

The *cmd* subscript denotes the commanded state, which comes from the outer loop control law. Natural frequency parameters of ω_n = 3 rad/sec and 2 rad/sec were used in the roll and pitch axes respectively, with damping ratio ζ = 0.9 in roll and 0.7 in pitch. The time constant parameter in the vertical axis was τ = 2 sec, while the yaw axis used τ = 0.4 sec.

The PID gains in Eq. (4) can be selected to acheive desired error dynamics based on natural fequency and damping parameters as discussed in detail in [10]. These can be tuned to acheive desired disturbance rejection and/or stability margins (as shown in [10]). In this study, the gains were set so the error dynamics have similar frequency properties as the command model responses discussed above.

3.2. Outer Loop Control Law

This paper develops fully autonomous control of the helicopter staring from a level flight approach, through descent, hover over the flight deck, and final descent to landing. This section describes the outer loop guidance law to acheive this goal. The helicopter is assumed to be initially flying at constant altitude, with an airspeed and heading that are reasonably close to the desired initial approach conditions (i.e. the controller does not set up the initial approach). It is assumed that the inertial coordinates of the helicopter *and the ship* are available to the controller. In addition, the heading and speed of the ship are known by the controller.

3.2.1. Coordinate Systems

Coordinate system definitions are critical for tracking motion relative to a moving flight deck. For the purposes of outer loop guidance and navigation, three sets of coordinate systems are used: flat earth inertial frame (with z axis up – a left handed NEU frame), ship heading frame (shf), and helicopter heading frame (hhf). The ship heading frame and helicopter heading frame are rotated from the NEU frame by a single rotation about the vertical axis (i.e. rotated by the ship or helicopter heading). The DCM only modifies x,y components of a vector when transforming between the three reference frames (vertical coordinates are the same in all frames). In addition, for the purposes of defining velocities and position, the ship frame is moving at steady speed and heading within the inertial frame.

3.2.2. Approach Path

The approach trajectory is parameterized by the range to the landing spot, and the decelerating descent is based on approach profiles observed for human rotorcraft pilots, as described in [11] and [12]. Relative approach speed is defined by the relationship:

$$V_{app} = \frac{\left(\frac{V_0}{2R_{pd}}\right)R}{\left(1 + \frac{R}{2R_{pd}}\right)} \tag{8}$$

where R is the range to the landing spot. The tunable constants, V_0 and R_{pd}, represent the asymptotic (i.e., initial) approach velocity and range at which the peak deceleration occurs, respectively. The approach path follows a constant relative glide slope, γ_{app}, and relative approach azimuth, ψ_{app}, such that the position and velocities in ship heading frame are governed by:

$$(9)\quad \begin{aligned} x^{shf} &= -R\cos\gamma_{app}\cos\psi_{app} & \dot{x}^{shf} &= V_{app}\cos\gamma_{app}\cos\psi_{app} \\ y^{shf} &= R\cos\gamma_{app}\sin\psi_{app} & \dot{y}^{shf} &= -V_{app}\cos\gamma_{app}\sin\psi_{app} \\ h^{shf} &= R\sin\gamma_{app} & \dot{h}^{shf} &= -V_{app}\sin\gamma_{app} \end{aligned}$$

These coordinates describe the position of the helicopter relative to the final hover point over the flight deck. A positive azimuth value indicates the helicopter is approaching from the starboard side of the ship. Since the ship frame is moving within the inertial frame, a constant value of a coordinate in the ship frame implies the aircraft is moving with the ship, while non-constant values imply a rate of closure or separation.

In previous work, an optimization study was conducted to understand the best ship approach path using this path parameterization [12]. Objective functions were formulated based on path tracking error, power consumption and fluctuations in thrust (due to the turbulent airwake). Constraints were applied on maximum pitch attitude and miminum clearance of the deck. This work provides guidance to the selection of the four path parameters r_{pd}, v_0, γ_{app}, ψ_{app}. For the present study, a few nominal cases will be shown to study performance of the controller, while detailed analysis of path are left to Ref. [12].

The position and velocities in Eq. 9 are transformed into the intertial NED reference frame. The altitude command in the intertial frame is offset by a bias to acheive a safe hover altitude at the end of the approach.

$$(10)\quad \begin{bmatrix} x_{N_{cmd}} \\ y_{E_{cmd}} \end{bmatrix} = \begin{bmatrix} \cos\psi_{ship} & -\sin\psi_{ship} \\ \sin\psi_{ship} & \cos\psi_{ship} \end{bmatrix} \begin{bmatrix} x^{shf} \\ y^{shf} \end{bmatrix} + \begin{bmatrix} x_{N_{ship}} \\ y_{E_{ship}} \end{bmatrix}_{filt}$$
$$h_{cmd} = h^{shf} + h_{ship_{filt}} + h_{bias}$$

Similar transformations are applied to the commanded velocities. Note that the position, altitude, and velocities of the ship flight deck are assumed to be known. These are added to the inertial position and velocity commands in the NEU coordinate system. However, on approach, it is not desired to track the dynamic motion of the flight deck due to sea state, so these values are filtered to yield an estimate of the steady flight deck trajectory due to ship course and heading. Details of the filter are shown in [2].

The airspeed at the end of the approach is relatively low, and the aircraft must fly with non-zero bank angle to trim in rectilinear flight. At low speeds there is insufficient aerodynamic force to balance lateral forces with sideslip and the helicopter must bank left. Transitions between coordinated flight (zero bank angle) at higher speeds to zero sidelip flight at low speeds can result in unwanted transients. Thus, the entire approach is performed in an uncoordinated flight mode. Bank angle is used to regulate lateral (cross track) velocity, and the heading is set to align with the velocity vector of the helicopter.

$$(11)\quad \psi_{cmd} = \operatorname{atan2}\left(\dot{y}_{cmd}, \dot{x}_{cmd}\right)$$

The approach profile is illustrated in Fig. 2. Note that the commanded heading of the helicopter is not the same as the relative approach azimuth, ψ_{app}, but results from the vector sum of the relative approach velocity vector and the ship's velocity. Similarly, the actual glide slope of the approach in the inertial frame will be less than the approach glide slope, γ_{app}.

3.2.3. Entry Approach Path

The entry to the approach path is achieved by ramping in the desired approach glide slope as the aircraft passes through a threshold range. This scheme effectively acheives a constant speed push-over maneuver to smoothly enter the descent. The vertical speed and altitude commands (in the ship frame) are governed by:

$$(12)\quad \begin{aligned} W_R &= \frac{R - R_{des}}{R_{init} - R_{des}} \\ \gamma_1 &= \left(1 - W_R\right)\gamma_{app} \qquad \gamma_2 = W_R \sin^{-1}\left(\frac{h_{init}}{R_{init}}\right) \\ V_Z^{shf}{}_{cmd} &= -V_{app}\sin\gamma_1 \qquad h_{cmd} = R\sin\left(\gamma_1 + \gamma_2\right) \end{aligned}$$

where R_{init} is the range to a point where the pushover is initiated, and R_{des} is the range to the point where the pushover is completed and the helicopter is in steady descent. These range parameters were set to 2000 ft and 1000 ft respectively, which resulted in a reasonable load factor during the push-over. Once the pushover is completed, the helicopter holds constant glide slope relative to the ship while decelerating according the profile in Eq. (8).

3.2.4. Path Following Control Law

On approach, the outer loop control is designed to track the flight path described in the previous

section. The flight path parameterization yields inertial positions, inertial velocities, and aircraft heading as described in Eq. (9) to Eq. (11). In addition, the inertial acceleration commands can be extracted from the velocity commands via differentiation (as long as the commands are smooth).

The roll and pitch axis control law in the outer loop is based on dynamic inversion (like the inner loop) but based on a very simple linear model of the translational dynamics. This simple model assumes that lateral and longitudinal accelerations in the helicopter heading frame are proportional to perturbations in roll and pitch attitude:

$$\dot{V}_x^{hhf} \approx -g\theta \qquad \dot{V}_y^{hhf} \approx g\phi \tag{13}$$

Applying the DI method with commanded attitudes as the plant input yields the control law:

$$\theta_{cmd} = -\frac{1}{g}\cdot\begin{pmatrix} K_{p\_xpos}(x_{cmd}^{hhf} - x^{hhf}) + K_{i\_xpos}\int (x_{cmd}^{hhf} - x^{hhf})\,\mathrm{dt} \\ +K_{d\_xpos}(V_{xcmd}^{hhf} - V_x^{hhf}) + \frac{d}{dt}\left(V_{xcmd}^{hhf}\right) \end{pmatrix} \tag{14}$$

$$\phi_{cmd} = \frac{1}{g}\cdot\begin{pmatrix} K_{p\_ypos}(y_{cmd}^{hhf} - y^{hhf}) + K_{i\_ypos}\int (y_{cmd}^{hhf} - x^{hhf})\,\mathrm{dt} \\ +K_{d\_ypos}(V_{ycmd}^{hhf} - V_y^{hhf}) + \frac{d}{dt}\left(V_{ycmd}^{hhf}\right) \end{pmatrix} \tag{15}$$

All measured and commanded x, y positions and velocities must be transformed from the inertial frame into the helicopter heading frame. The commanded velocities come directly from the time derivative of the command flight path as shown in Eq. (9). As such, the controller effectively follows the velocity profile described by Eq. (8).

Heading and altitude control are also included in the outer loop. These use basic PI compensation on the altitude and heading error to yield commanded vertical speed and yaw rate respectively. The altitude controller also uses a feedforward term equal to the vertical acceleration defined by the commanded flight path.

Note that the approach path in Eq. (9) is parameterized by range to the flight deck, *R*. When coming in directly from the stern (ψ_{app} = 0), the *x* position compensation in Eq. (14) has negligible effect during the approach. In this case, the commanded *x* position is *R**cos(γ_{app}), while the aircraft *x* position is defined by: *R**cos(γ_{app} + $\Delta\gamma_{app}$), where $\Delta\gamma_{app}$ is the glide slope error. The cosine terms are nearly equal unless there is a very large glide slope error. In direct stern approaches, the x-axis control law primarily serves to regulate approach velocity (Eq. (8)), while glide slope and cross track correction are achieved by the vertical and lateral axes. With non-zero azimuth, the x-position compensation does play a role, working with y-position compensation to correct cross track, and all position compensation is active when regulating position around the final hover point.

3.2.5. Station-keeping and Landing

Once the helicopter reaches a hover over the ship flight deck within tolerances, it enters a station-keeping mode. In this mode, the helicopter tracks the x, y location of the center of the flight deck and it holds a constant relative height above the deck. Since the outer-loop controller operates on commanded x, y position, the exact same control law is used in final station-keeping as on the approach, which avoids transients associated with switching of control laws.

Depending on the landing strategy used (as described in Section 5) the controller can either filter out most of the dynamic deck motion (essentially hold steady altitude and an inertial velocity that matches the ship course), or it can track the dynamic motion of the deck due to sea state. This is achieved by varying a frequency parameter in the deck motion filter discussed in section 3.2.2 and Ref. [2]. The choice of landing strategy depends on whether or not deck motion prediction algorithms are used.

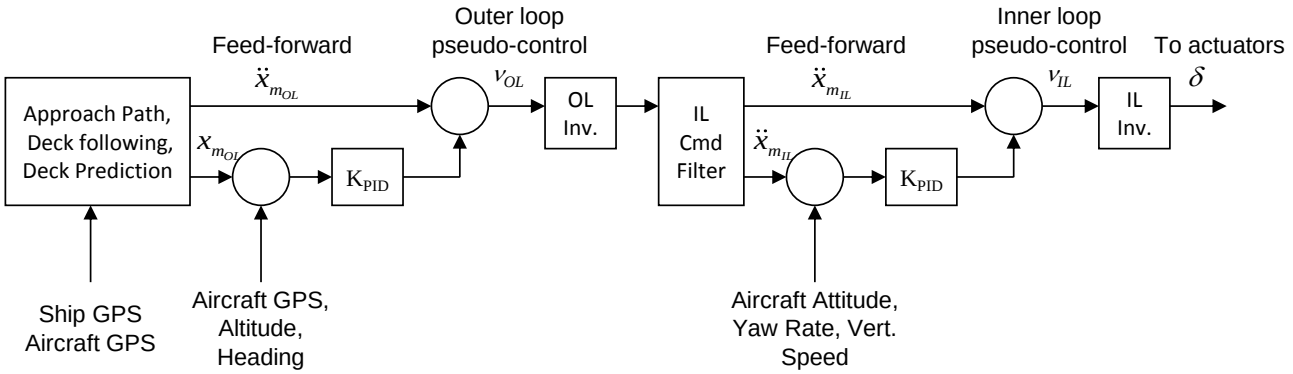

Fig. 1 Control Law Schematic

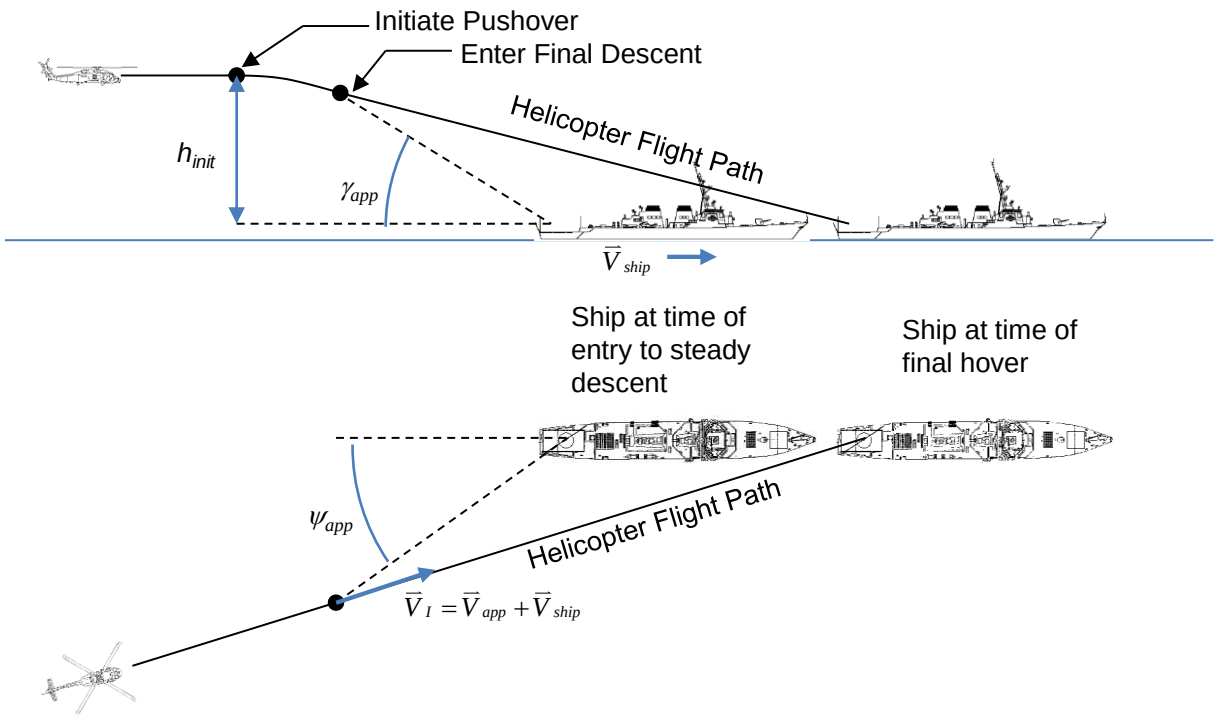

Fig. 2 Approach Path

4. DECK MOTION PREDICTION

The purpose of the deck motion prediction is to provide an estimate of future deck state, so that the controller can effectively time the landing and match relative velocity at touchdown. It is assumed that full 6-DOF measurement of the deck state is available, but there is no information on the sea conditions or approaching waves. A data-driven method is used, where past history of deck inertial states are the only measurements used in the prediction. The algorithm estimates a short-term response based on observed patterns in the quasi-periodic motion of the deck. In the present study, only the *x*, *y*, *z* inertial positions of the deck are used in the prediction (deck Euler angles will be considered in future work).

A minor component analysis (MCA) method [13] was used for deck motion prediction. The statistical method for extracting a minor component from the input data is called minor component analysis. The MCA determines the directions of smallest variance in a distribution. They correspond to the directions of those eigenvectors of the covariance matrix of the data which have the smallest eigenvalues. The main idea of MCA was applied for a curve fitting problem. Given a set of data points ($\mathbf{x_1}$, $\mathbf{x_2}$), the search for a line model to fit the data in the usual least square sense becomes the problem of finding a pair of estimates. If it is assumed that only the measurements $\mathbf{x_2}$ contain errors while the measurements $\mathbf{x_1}$ are accurate, the total least squares approach gives the optimal way to minimize the sum of the squared lengths of all the bars which are perpendicular to the estimated line. The total least squares fitting problem can be reduced to the problem of finding the minimum eigenvalue and its corresponding normalized eigenvector of matrix or, in other words, finding the first minor component of the data set.

To implement the MCA method, a set of ship motion data are aligned into a sequence of vectors, $\boldsymbol{X_i}$. The eigenvalues and eigenvectors of the autocorrelation matrix, $\boldsymbol{R} = \sum_{i=1}^{N} X_i X_i^T$, can then be calculated. The vector $\boldsymbol{X_i}$ is formed as $[\boldsymbol{X_{1i}}, \boldsymbol{X_{2i}}]^T$. where $\boldsymbol{X_{1i}}$ is the measured ship motion and $\boldsymbol{X_{2i}}$ is the forecasted motion in the length of the forecasting window. Based on the MCA algorithm, the forecasted vector ($\boldsymbol{X_{2i}}$) is calculated using an approximated equality formulation consisting of eigenvectors which are associated with the smallest eigenvalues of the autocorrelation matrix ($\boldsymbol{R}$).

The MCA based forecasting algorithm was tuned and evaluated using a set of ship motion data with full 6-DOF motion (surge, sway, heave, roll, pitch, and yaw). Time histories were generated for ship hulls similar to the DDG-51 and LHA class ships in response to various sea state wave conditions, wave heading angles, and ship speeds. The statistical prediction errors were evaluated using over 1,000 test cases. Each set of test conditions was a combination of (a) three sea states (3, 5, and 6), (b) two ship speeds (10 and 20 knots), (c) ten wave

heading angles (0, ±30, ±60, ±90, ±135, 180 degrees), (d) five significant wave heights for each given sea state, and (e) four wave modal periods for each given sea state.

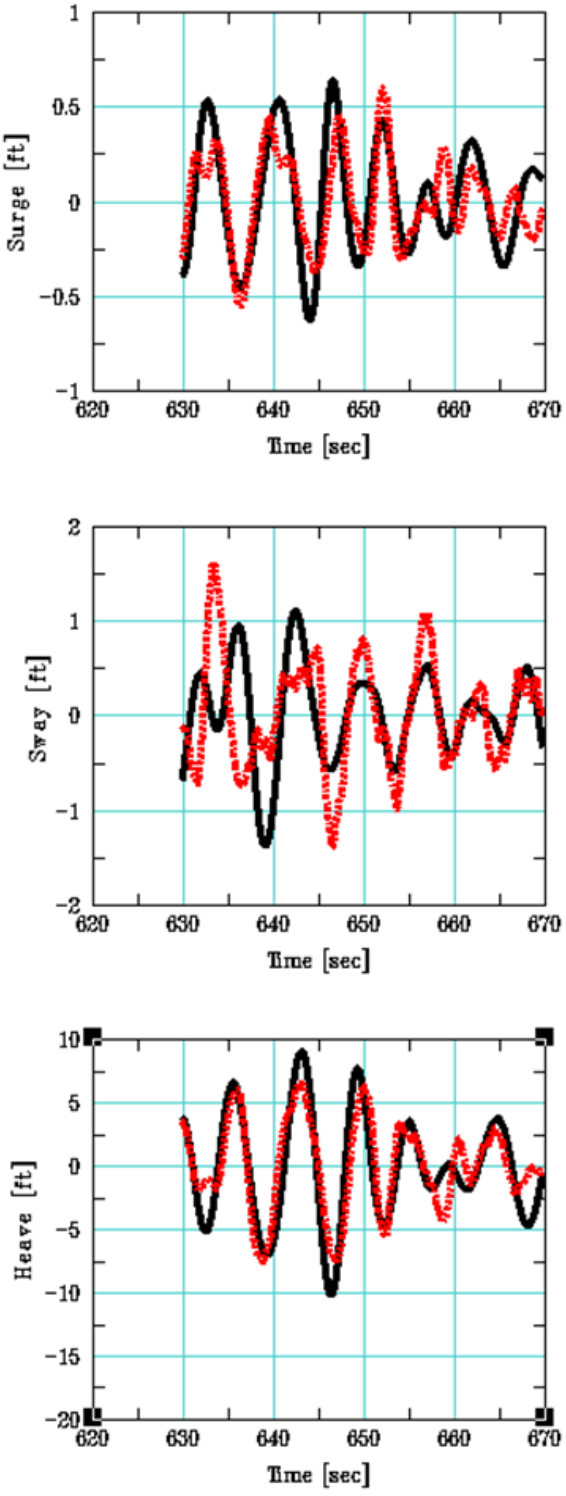

Fig. 3 Deck Motion Prediction Performance

The MCA based ship motion forecasting algorithm was designed to predict the deck motion up to 6 seconds in the future. The deck motion is sampled at a 10 Hz rate, and the MCA algorithm uses the past 1,500 samples (150 seconds) of deck motion history in the prediction. The minor components of the autocorrelation matrix were selected in a sense that their energy added up to no more than 1% of the total energy. These choices were based on both the statistical analysis of the prediction accuracy and the computational complexity, such that the computations can be readily made in real-time. Note that the data used in the tuning and evaluation of the MCA algorithm was not the SCONE ship motion data (the SCONE data was used in the final simulation results shown in the following sections).

Fig. 3 shows a sample time history comparison using data for a ship similar to the DDG-51. The plot shows actual ship motion (black solid lines) and forecasted motion (red dashed line) with sea state 5, ship speed of 20 knots, and a wave heading angle of 0 degrees. The prediction horizon was set to six seconds, and the forecasted values are shifted back in time by six seconds to provide direct comparison with the actual deck motion.

5. LANDING PHASE

The objective of the landing phase is to take the helicopter from a stable hover over the flight deck to touchdown on the flight deck, with all three landing gear contacting the deck at acceptable relative velocity. The purpose of this research is to develop methods that allow landings in high sea state conditions. Thus, for the purposes of simulation evaluation, the landing control does not attempt to wait for a quiescent period in the ship motion (although clearly a practical system would need to observe some operating limits on deck motion).

Two approaches were investigated for the autonomous landing phase. The first method is a simple approach that attempts to follow the measured deck motion during the entire landing phase. This is considered the baseline case, and does not use the deck motion prediction algorithms discussed in the previous section. While the approach was shown to have reasonable performance for these simulations, it is not considered an ideal approach, as the helicopter must undergo much unnecessary maneuvering during the descent if the flight deck is experiencing large dynamic motion.

A more desirable approach is to time the landing so that the helicopter approaches the deck smoothly but terminates with an acceptable relative velocity. To achieve this timing, the deck motion prediction

algorithms are used with an optimal control scheme.

5.1. Simple Descent with Deck Tracking

The station-keeping control laws of Eq. (14) and (15) are used throughout the landing phase. In this case, the commanded (x, y) positions and velocities are simply equivalent to the measured (x, y) positions and velocities of the flight deck.

The vertical axis controller uses the measured altitude and vertical velocity of the flight deck with a constant descent bias of 1.5 ft/sec. The commanded altitude simply uses the integrated velocity command.

$$V_{Z_{cmd}} = V_{Z_{fd}} - V_{descent}$$
$$h_{cmd} = h_{bias} + h_{fd} + \int V_{Z_{cmd}} dt \quad (16)$$

where the subscript *fd* denotes the center of the flight deck.

5.2. Optimal Control Strategies with Deck Motion Prediction

This algorithm uses optimal control theory to plan a descent path to the center of the landing deck such that the final vertical and lateral velocities match that of the deck at the expected touchdown time. The same outer-loop guidance control laws are used, but the commanded lateral and vertical positions and velocities (in the ship heading frame) are generated by the optimal control law. The x position and velocity in the ship heading frame still track the current deck position as in the previous method.

The optimal control scheme is based on the simple dynamics of a 1 DOF inertial system:

$$\dot{y} = v$$
$$\dot{v} = a(t) \quad (17)$$

This is a second order system with states *y* and *v* (position and velocity), and the control input *a* (acceleration). Note that the DI method effectively de-couples the four control axes, and the outer loop control scheme is well-suited to follow acceleration commands. Thus, Eq. (17) is a reasonable model for the lateral, longitudinal, or vertical outer loop commands, where *a* is the feed-forward acceleration command, *v* is the commanded velocity, and *y* is the commanded position (e.g. as seen in Eq. (14) and (15) of the lateral and longitudinal outer loop control laws).

We then seek a control law for $a(t)$ that takes the helicopter from current state $y(t_0)$ and $v(t_0)$ to a terminal state at a fixed time horizon $y(t_f)$ and $v(t_f)$. The time t_f is the prediction horizon of the deck motion prediction algorithm and the time to land. The terminal states are set to match the predicted deck state at the landing time. During the landing maneuver, the prediction horizon is shortened and the predicted deck state updated. The control law is derived from the classical optimal control problem that minimizes the following objective function [13]:

$$J = \tfrac{1}{2}c_1\left[v(t_f) - v_d\right]^2 + \tfrac{1}{2}c_2\left[y(t_f) - y_d\right]^2 + \tfrac{1}{2}\int_t^{t_f} a^2 dt \quad (18)$$

where v_d and y_d are set to match the forecasted deck state at touchdown. Thus the objective function minimizes a weighted function of terminal error and integrated control effort. In the case of vertical velocity, we add a negative bias to the terminal velocity of -1.5 ft/sec, to ensure that the helicopter descends down to wheel contact (rather than hover just over the deck).

The resulting control law is of the form:

$$a(t) = -\Lambda_v(t)\left[v(t) - v_d\right] - \Lambda_y(t)\left[y(t) - y_d\right] \quad (19)$$

where Λ_v and Λ_y are time-varying gains defined in Ref. [14]. The velocity and position weighting factors selected were, $c_1 = c_2 = 5$. This control law yields a commanded acceleration for both the lateral and vertical axes. The acceleration is integrated twice to yield commanded velocity and positions that are fed to the outer loop guidance law.

In order to avoid infeasible landing trajectories, the landing profile (in terms of accelerations, velocities, and positions) is calculated before initiating the landing sequence. The commanded accelerations and velocities must be within the following tolerances before initiating the landing:

$$|a_y(t)| \le 0.2g, \; |a_z(t)| \le 0.3g$$
$$|v_y(t)| \le 4 \text{ ft/sec}, \; |v_z(t)| \le 6 \text{ ft/sec} \quad (20)$$

In addition, the altitude profile is checked against forecasted deck altitude to verify that it will not make early deck contact. Once these tolerances are satisfied, the five second landing sequence is initiated. The target landing position and speed are updated every 0.096 seconds based on the latest deck forecast data from the MCA algorithm.

6. RESULTS

Numerous simulation cases were run in FLIGHTLAB, and sample simulation results are shown in the following sections. For clarity, separate results are shown for the approach phase and the landing phase (integrating the approach and

the landing is relatively straightforward and has been achieved, but results are not shown here).

6.1. Approach

As discussed in Section 3.2.2, the approach is defined by the parameters: R_{pd}, V_0, γ_{app}, and ψ_{app} – the range to peak deceleration, asymptotic approach velocity, glideslope, and azimuth. Numerous variations in the approach parameters have been tested in previous work [12], but only a few cases are shown here in order to study the control law performance. In all cases shown, the velocity and glide slope parameters are V_0 = 125 ft/sec and γ_{app} = 8°. The deceleration parameter, R_{pd} = 300 ft, for most of the cases shown. In all cases, the ship is moving forward at 20 knots.

Fig. 4 shows the approach trajectories in inertial coordinates for two different azimuths, ψ_{app} = 0° (straight in approach), and ψ_{app} = 45° (a diagonal approach from the starboard). Fig. 5 shows a close up top view of the trajectory in the final phase of the approach. Results show the controller can achieve a successful approach profile for both stern (i.e., straight-in) and oblique approaches.

Fig. 6 shows the actuator control activity during the approach with ψ_{app} = 0°. The actuator motion is well within travel limits, with the largest motion being due to the change in trim (from about 80 knots to 20 knots over the flight deck).

Fig. 7 shows the aircraft velocities in the inertial frame (+ North, East, and Up). The commanded velocities are shown with the blue dashed line. These commands are a summation of the approach profile, and filtered measurements of the flight deck velocity. Note that the commanded velocities shown in the plot are in the ship heading frame, while aircraft velocities are in NEU frame. In these simulations the predominant ship heading is North with some small dynamic yaw oscillations. Thus, the ship heading frame is nearly aligned with the NEU inertial frame. However, at the beginning of the simulation, small yaw oscillations of the ship result in significant lateral velocity commands when the approach velocity vector is transformed into the inertial frame. This produces the lateral velocity oscillations at the beginning of the simulation. Future implementations will apply filtering to the ship heading used in transformations. The oscillations in the last phase of the approach are commanded by the dynamic oscillation of the ship as the helicopter performs station-keeping over the flight deck.

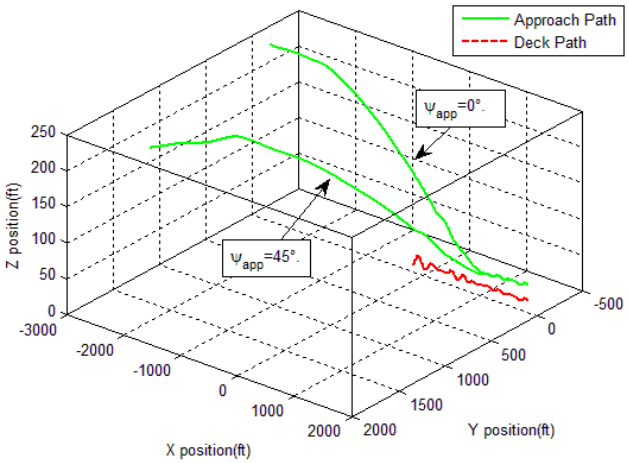

Fig. 4 Approach trajectory from 0° and 45° azimuth

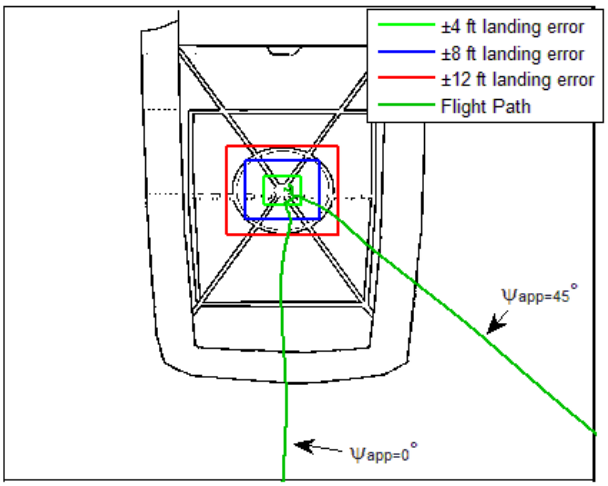

Fig. 5 Final approach from 0° and 45° azimuth

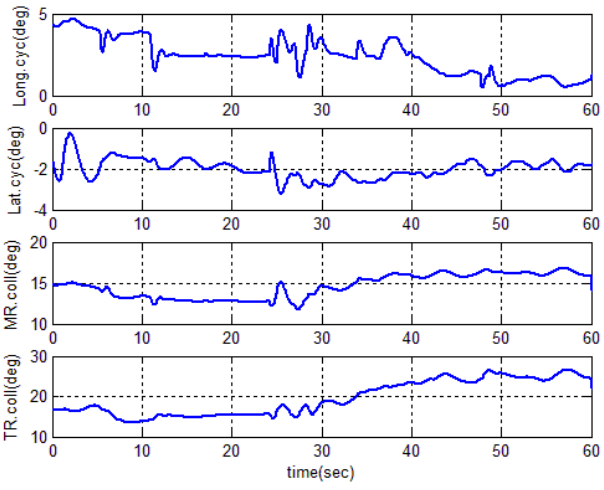

Fig. 6 Control activity during approach, ψ_{app} = 0°

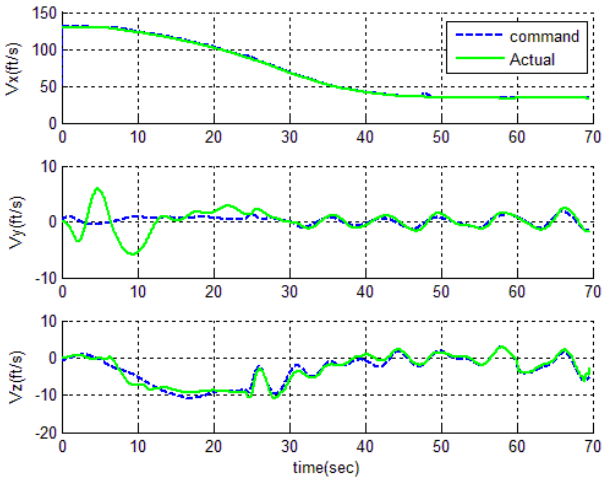

Fig. 7 Velocities during approach, ψ_{app} = 0°

The range to peak deceleration parameter, R_{pd}, governs the aggressiveness of the deceleration at the end of the approach. Lower values of R_{pd} cause the helicopter to decelerate over shorter distance. Fig. 8 shows the altitude profile at the end of the approach for two cases with ψ_{app} = 0°. The baseline case uses R_{pd} = 300 ft, and the more aggressive aproach uses R_{pd} = 200 ft. Results show that the control law performance is sensitive to this parameter. The results show that both cases result in some undershoot of the commanded altitude profile as the helicopter is arresting both its forward speed and descent rate. However, the more aggressive case results in a significantly larger altitude error (almost 20 ft). The aggressive deceleration also resulted in a high pitch attitude (approaching 14° nose up), which positions the tail wheel dangerously close to the flight deck.

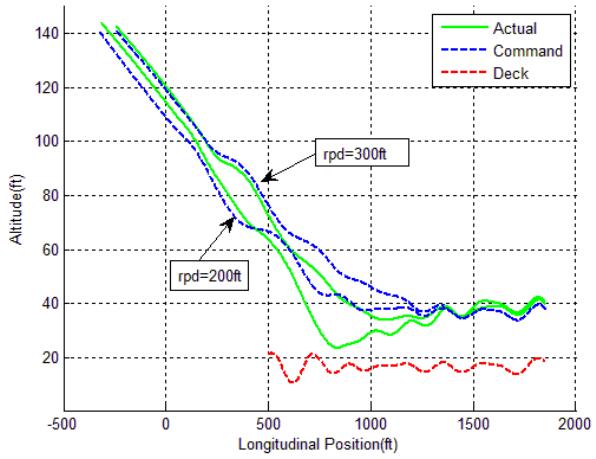

Fig. 8 - Final altitude tracking during approach (ψ_{app} = 0°, R_{pd}= 200 ft and R_{pd}= 300 ft)

6.2. Landing with Deck Tracking

Landing results were generated with using a simple descent maneuver while tracking the center of the deck in the x and y axes. During descent, the helicopter maintains a steady *relative* descent rate, tracking the deck heave motion throughout. The simulations start at a stationary hover 20 ft over the flight deck, and then initialize a descent after 10 seconds. The simulation is completed when all three landing gear are in contact with the deck (at which point collective is lowered to its minimum setting). Fig. 9 shows a sample trajectory. The red vertical lines indicate time of deck contact (first the tail gear, followed by the left and right gear shortly afterwards). The results also show the helicopter climbs and descends three cycles during the process.

Thirty randomized cases were generated by initiating the simulation at different times in the deck motion time history, and randomizing the airwake turbulence. Fig. 10 shows a scatter of the landing location relative to tolerance boundaries for ±4 ft, ±8ft, and ±12 ft. It successfully lands within the smallest tolerances in all 30 cases, with an average landing error less than 1 ft. Fig. 11 shows sink rate and lateral velocity with respect to the flight deck of each of the landing gear upon first deck contact, along with tolerance boundaries: 2 ft/sec, 4 ft/sec, and 6 ft/sec. 63% of the cases were within the green boundary, 87% within the blue boundary, and all cases within the red boundary.

These performance results exceeded expectations for this simple landing procedure operating with relatively large deck motion. It was expected that the controller would have difficulty tracking the large deck motions. However, at this point in the study, the aircraft simulation and control assumptions are relatively ideal: fast actuators and no significant transport delay due to sensors or sample rates. Thus, additional analysis was conducted with added transport delay.

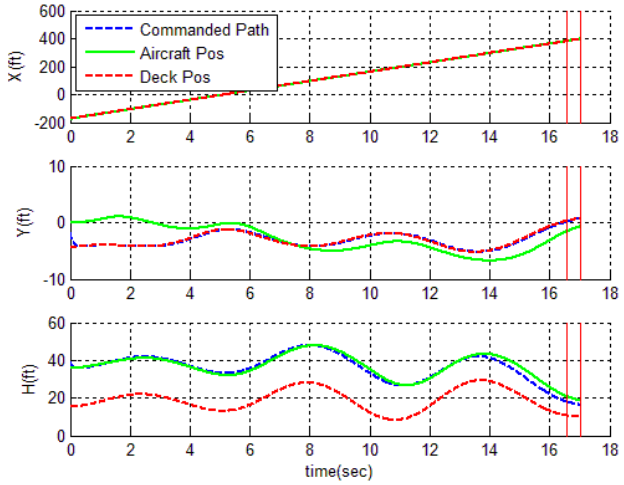

Fig. 9 Sample landing trajecory

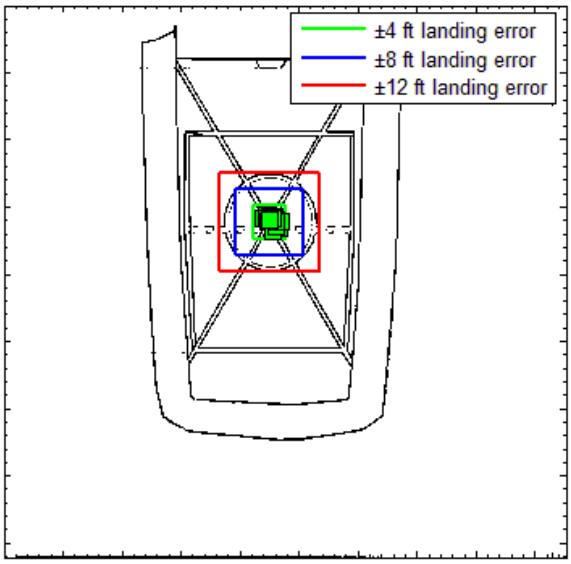

Fig. 10 Landing position scatter

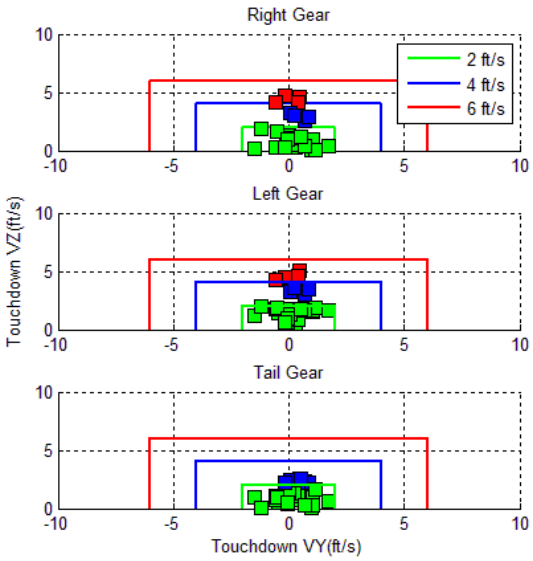

Fig. 11 Landing velocity scatter

Fig. 12 and Fig. 13 show landing results with a 0.200 sec transport delay added to the ship inertial position sensor, to model expected time delays in the measurement and transmission of the deck state to the aircraft control system. As expected, the time delay degrades performance, but not dramatically. The longitudinal landing location is biased toward the aft part of the landing for the simple reason that the ship is moving forward at 20 knots, and a delayed measurement results in a consistent 7 ft bias to the x measurement. This could readily be compensated for if the ship speed is known. Lateral position error is still largely within the ±4 ft tolerance with the exception of one case. The touchdown velocity shows some degradation, with at least one gear outside of the green tolerance boundary in 63% of the cases. However, only 10% of the cases are outside of the blue boundary and none of the cases are outside of the red boundary.

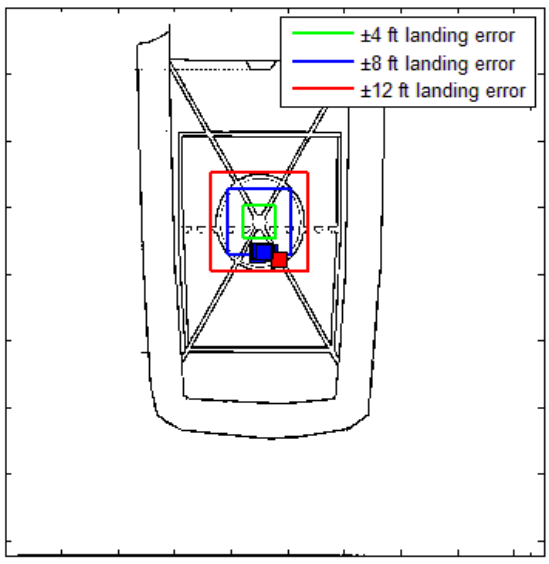

Fig. 12 Landing position scatter, 0.2 sec time delay

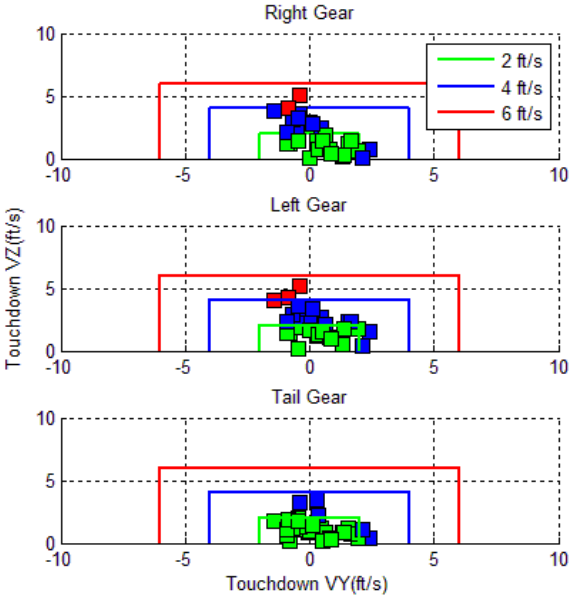

Fig. 13 Landing velocity scatter, 0.2 sec time delay

Landings were also evaluated at a higher gross weight (20,000 lbs) with mass moments of inertia scaled by the increase in weight (an 18% increase). The linear models in the control law were not modified (i.e. they still represented the 17,000 lbs helicopter). As expected, the peformance degraded but only slightly. Only one case (3.3%) exceeded the green boundaries (±4 ft) for position error on touchdown. There were more cases where the lateral or vertical touchdown velocity of at least one landing gear did not meet the desired tolerance. In 53% of the cases, the green boundary (2 ft/sec) was exceeded, but in only one case (3.3%) was there a velocity outside of the blue boundary (but still within the red boundary). Power required was also recorded during these simulations. The maximum power observed was 2610 shp, which is well within

the expected power limitations of a helicopter of this type. The results also demonstrate the robustness of the DI controller, since plant models and the controller design were not updated to reflect the higher weight and inertias.

6.3. Landing using Optimal Control with Deck Motion Prediction

Preliminary landing simulations were conducted using the optimal predictive landing method described in 5.2. Fig. 14 shows a sample landing trajectory that was successful. The landing sequence was initiated at 11.3 seconds into the simulation. As seen in the figure, the helicopter is commanded to hold a stable inertial hove over the landing deck until the landing maneuver begins. It then performs a more direct descent rather than follow the deck motion. The figure shows the predicted deck motion as generated by the MCA algorithm as the magenta line. The curve is shifted forward in time by the prediction horizon, which is 5 seconds for most of the simulation. At about 16.3 seconds these values "bunch up", as the forecast time is shortened throughout the descent maneuver. There is some significant error in the deck motion prediction, notably in the *y* position. But as the forecast time decreases, the prediction becomes more accurate, as shown by the magenta prediction line moving closer to the actual deck position shown by the red line.

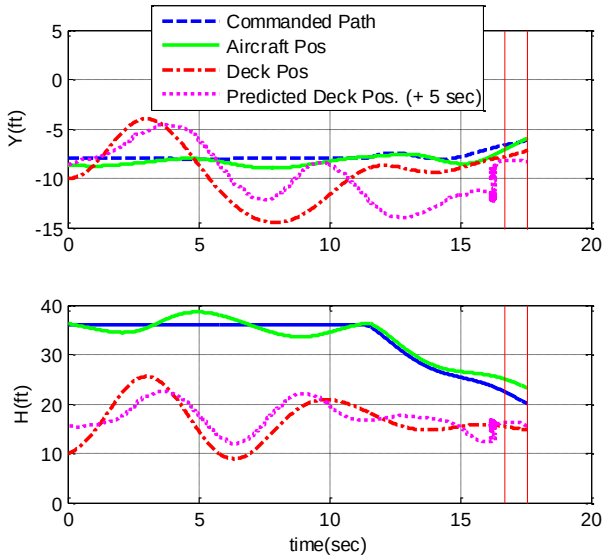

Fig. 14 Sample landing trajectory with optimal predictive landing control law

For this case, the final x, y errors at touchdown were within the desired tolerances (0.9 ft, and 1.2 ft respectively). The vertical touchdown velocities of the front landing gear were slightly higher than desired (2.4 ft/sec) while the lateral velocity relative to the deck was only 0.3 ft/sec. While this particular case was relatively successful, the optimal predictive landing method has generally been found to perform less consistently than the simple landing method described in 5.1. In certain cases, phase errors in the heave motion prediction cause the helicopter to make deck contact too early, resulting in hard landings with sink rates as high as 10 ft/sec. Development and improvement of the control and prediction algorithm is ongoing. Based on preliminary results, it appears this controller is sensitive to inaccuracy in the forecasting algorithm.

7. CONCLUSIONS

This paper presented the design and simulation testing of a control law for autonomous recovery of a rotorcraft to a moving ship with focus on the final approach, descent, and landing phases of the ship recovery task. The controller is tested using FLIGHTLAB simulations of a medium utility helicopter operating to a destroyer class ship. The dynamic inversion method was applied for inner loop and outer loop compensation. A parameterized approach profile was implemented, which was derived based on typical approach profiles of human pilots. Two landing methods were investigated. One method attempted to follow the dynamic motion of the deck while steadily closing the vertical offset at 1.5 ft/sec until deck contact. The second method used a deck motion prediction algorithm that forecasts future deck state up to 5 seconds in the future. The method uses an optimal control scheme to match deck position and velocity after a 5 second descent. The following conclusions can be made regarding the design effort to date:

1. With appropriate coordinate transformations and a well-defined path parameterization, the approach control problem proved to be relatively straightforward. It is important that the path be smooth, kinematically consistent, and not overly aggressive. Results showed that in some cases, the ship coordinate transformation using instantaneous ship heading resulted in large lateral velocity commands, and these should be filtered in future implementations.
2. A deck motion prediction algorithm using the MCA method was developed and tested for a variety of ship motion cases. Results showed reasonably accurate predictions of all 6 DOF for forecast times up to six seconds.
3. The simple landing control scheme that tracked the measured deck motion worked surprisingly well with the current simulation and control scheme. The DI controller also proved to be effective at tracking relatively large deck dynamic motion with minimal phase delay. Thus, there were no issues with this approach.

Even with a 0.2 second time delay the approach appeared feasible. The controller also proved to be robust to higher mass and inertia properties. More testing should be conducted to study the effects of slower actuation, additional time delay, sensor noise, and more restrictive power and torque limits.

4. The deck tracking scheme used in the simple landing controller can result in unnecessary maneuvering when landing on a dynamic flight deck. For example, the aircraft can perform multiple climbs and descents while tracking a heaving deck. However, if the aircraft has the power and control authority to perform these maneuvers, it appears to be a viable control scheme.
5. The optimal predictive landing method is still under development, but in its current form the method is less reliable than the simple landing scheme, with vertical landing speeds as high as 10 ft/sec. The controller is sensitive to errors in the predicted deck motion. However, when successful, the landing trajectories are much less dynamic than the deck tracking approach. Thus further investigation is warranted.
6. Current implementation of the deck tracking and deck prediction methods do not make use of the deck attitude. Using this information in the control law might be used to better match the aircraft and ship attitudes at contact. This should be investigated in future work.

8. ACKNOWLEDGEMENT

This work was sponsored by the Office of Naval Research, ONR, under contract number N00014-14-C-0004. The views and conclusions contained herein are those of the authors and should not be interpreted as necessarily representing the official policies or endorsements, either expressed or implied, of the Office of Naval Research, or the U.S. government.

9. REFERENCES

[1] Perrins, J. A., and Howitt, J., “Development of a pilot assisted landing system for helicopter/ship recoveries,” American Helicopter Society 57th Annual Forum Proceedings, Washington, DC, May 2001.

[2] Soneson, G.L., and Horn, J.F., “Simulation Testing of Advanced Response Types for Ship-Based Rotorcraft,” Proceedings of the American Helicopter Society 70th Annual Forum, Montreal, Canada, May 2014.

[3] Voskuijl, M., Padfield, G., Walker, D., Manimala, B., Gubbels, A., “Simulation of automatic helicopter deck landings using nature inspired flight control and flight envelope protection.” *Aeronautical Journal* 114(1151): Paper No. 3426, 2008.

[4] Yidong Yang and Suozhong Yuan, *Guidance and Control of Unmanned Helicopter Ship Landing*, Defense Industry Press, Beijing, Oct. 2013.

[5] Hu, B., Lu, L., and Mishra, S. “A control architecture for fast and precise autonomous landing of a VTOL UAV onto an oscillating platform,” American Helicopter Society 71st Annual Forum Proceedings, Virginia Beach, VA, May 2015.

[6] Peters, D. A. and He, Chengjian, “Finite State Induced Flow Models Part II: Three Dimensional Rotor Disk," *AIAA Journal of Aircraft*, Vol. 32, No. 2, March-April, 1995

[7] He, C., Goericke, J., and Hao, K., “Modeling Enhancements for Physics-Based Simulation Validations," Proceedings of the American Helicopter Society 61st Annual Forum, Grapevine, TX, June 2005.

[8] Schwartz, A., “Systematic Characterization of the Naval Environment (SCONE) – Standard Deck Motion Data for a Generic Surface Combatant,” Memorandum from Office of Naval Research and Naval Surface Warfare Center - Carderock Division, May 2015.

[9] Xin, H. and He, C., “A Statistical Turbulence Model for Shipboard Rotorcraft Simulations," Proceedings of the American Helicopter Society 63rd Annual Forum, Virginia Beach, VA, May 2007.

[10] Zheng, A. and Horn, J.F., “Investigation of Bandwidth and Disturbance Rejection Properties of a Dynamic Inversion Control Law for Ship-Based Rotorcraft,” American Helicopter Society 71st Annual Forum Proceedings, Virginia Beach, VA, May 2015.

[11] Heffley, R. K., “A Model for Manual Decelerating Approaches to Hover,” 15th Annual Conference on Manual Control Proceedings, Air Force Flight Dynamics Laboratory, Dayton, OH, November 1979, pp. 545–554.

[12] Tritschler, J.K., Horn, J.F., and He, C., “Objective Function Development for Optimized Path Guidance for Rotorcraft Shipboard Recovery,” AIAA Atmospheric Flight Mechanics Conference, Dallas, TX, June 2015.

[13] Oja, E., “Principal Components, Minor Components, and Linear Neural Networks,” *Neural Networks*. Vol. 5, pp.927-935, 1999.

[14] Bryson Jr., A. E., and Ho, Y.C., *Applied Optimal Control: optimization, Estimation, and Control,* Revised Printing, Hemisphere Publishing, Washington, D.C., 1975, pp.154-155.